2007

Electromagnetic strong plasma turbulence

A. Melatos
University of Melbourne

Frederick A. Jenet
The University of Texas Rio Grande Valley

P. A. Robinson
University of Sydney

Electromagnetic strong plasma turbulence

A. Melatos
School of Physics, University of Melbourne, Parkville, VIC 3010, Australia

F. A. Jenet
Department of Physics and Astronomy, University of Texas at Brownsville, Brownsville, Texas 78520

P. A. Robinson
School of Physics, University of Sydney, Sydney, NSW 2006, Australia

(Received 17 October 2006; accepted 11 January 2007; published online 28 February 2007)

The first large-scale simulations of continuously driven, two-dimensional electromagnetic strong plasma turbulence are performed, for electron thermal speeds $0.01c \leqslant v \leqslant 0.57c$, by integrating the Zakharov equations for coupled Langmuir and transverse (T) waves near the plasma frequency. Turbulence scalings and wave number spectra are calculated, a transition is found from a mix of trapped and free T eigenstates for $v \geqslant 0.1c$ to just free eigenstates for $v \leqslant 0.1c$, and wave energy densities are observed to undergo slow quasiperiodic oscillations. © *2007 American Institute of Physics*. [DOI: 10.1063/1.2472293]

Bursts of electromagnetic (EM) radiation at the plasma frequency ω_p and harmonics, coexisting with electrostatic (ES) noise and quasineutral density wells, are often observed in beam-plasma[1–3] and ionospheric-heating[4,5] experiments in the strong-plasma-turbulence (SPT) regime $W = \epsilon_0 \langle |\mathbf{E}|^2 \rangle / 4 n_0 k_B T_e \gtrsim (k \lambda_D)^2$, where $\langle |\mathbf{E}|^2 \rangle^{1/2}$ is the rms electric field strength, n_0 is the mean electron density, T_e is the electron temperature, k is the characteristic ES wave number, and λ_D is the Debye length. One application of EMSPT is to experiments where an ultrashort laser pulse is fired into an underdense plasma, generating slow-moving, long-lived EM wave packets.[6–8] It is also relevant to inertial confinement fusion research, e.g., at the National Ignition Facility and Laser Megajoule facility, where $T_e \approx 80$ MK.[9] Considerable ingenuity is needed to suppress hydrodynamic instabilities at these facilities, and EMSPT can disrupt symmetry of imploding fuel capsules by converting some laser power to free EM waves near ω_p, and fast electrons via transit-time interactions,[10,11] which redistribute energy unevenly in laser hot spots.[9]

Theoretical investigations of ESSPT have yielded detailed understanding of its nonlinear dynamics (e.g., ponderomotive self-focusing and collapse), wave-energy scalings (e.g., versus driver parameters), and wave spectra.[10,12,13] EMSPT has been studied less.[4–8,14–22] Many of its properties are poorly understood, including the spatial structure of the turbulence, how ES waves trapped in density wells are converted to free EM waves, and EM back reaction on the dynamics. Simulations of ionospheric heating are also incomplete, because turbulence is evolved electrostatically although an EM driver is used, and EM radiation is calculated perturbatively without including trapped radiation and its back reaction.[4,5]

In this letter, we report simulations of two-dimensional (2D) EMSPT in which coupled ES Langmuir (L) modes and EM transverse (T) modes evolve self-consistently. The simulations, on a 256^2 grid, are the first to produce a turbulent state with many ($\gtrsim 10^2$) wave packets simultaneously present (hence good statistics), cover a wide range of electron thermal speeds $0.01c \leqslant v = (k_B T_e / m_e)^{1/2} \leqslant 0.57c$, be continuously driven to a statistically steady state, explore dependencies on damping and driver parameters, and reveal low-temperature T-wave delocalization. Previous simulations were limited to a 64^2 grid containing $\leqslant 3$ packets at a time, and to an undriven case with $v = 0.08c$.[21] Analytic work has been restricted to $v \ll c$, $\omega \approx 2\omega_p$ where a wave packet radiates as an antenna and the back reaction of T waves is slight,[14–16] or to the weak-turbulence regime $W \ll (k\lambda_D)^2$,[20] and always for a single packet rather than a turbulent ensemble.[14–16,18,19]

In the absence of a zeroth-order magnetic field, EMSPT is approximately described by the EM Zakharov equations[10,18,19,22] for the slowly varying L-T electric-field envelope $\boldsymbol{\mathcal{E}}(\mathbf{x},t)$,

$$i \frac{\partial \boldsymbol{\mathcal{E}}}{\partial t} = \left(\frac{v_T^2}{2\omega_p} \nabla \times \nabla \times - \frac{v_L^2}{2\omega_p} \nabla \nabla \cdot + \frac{\omega_p \delta n}{2 n_0} - i \hat{\gamma}_L \right) \boldsymbol{\mathcal{E}}, \tag{1}$$

defined by $\mathbf{E} = \boldsymbol{\mathcal{E}} e^{-i\omega_p t}$, and for the slowly varying, ion-sound like (S), quasineutral density perturbation $\delta n(\mathbf{x},t)$,

$$\left(\frac{\partial^2}{\partial t^2} + 2\hat{\gamma}_S \frac{\partial}{\partial t} - v_S^2 \nabla^2 \right) \frac{\delta n}{n_0} = \frac{\epsilon_0}{4 n_0 m_i} \nabla^2 (|\boldsymbol{\mathcal{E}}|^2), \tag{2}$$

with $v_S^2 = (1 + 3T_i/T_e)(m_e/m_i)v^2$, $v_L^2 = 3v^2(1+\xi/5)/(1+5\xi+\xi^2)$, $v_T^2 = c^2(1+6\xi+6\xi^2/5)/(1+5\xi+\xi^2)$, $\omega_p^2 = (n_0 e^2/m_e \epsilon_0)(2+\xi)/(2+6\xi+3\xi^2)$, and $\xi = v^2/c^2$. We approximate relativistic expressions for v_L and v_T here by Padé formulas,[23] but neglect the relativistic ponderomotive terms in (2), which tend to be significantly smaller than the ones retained (the results should be viewed as semiquantitative due to this neglect and the approximations inherent in the Zakharov equations, which neglect second-harmonic effects and thus also require $k^2 v_T^2, k^2 v_L^2 \ll \omega_p^2$), the operators $\hat{\gamma}_L(\mathbf{x},t)$ and $\hat{\gamma}_S(\mathbf{x},t)$ describe L and S damping and growth, and T waves are not damped/driven directly. We study the regime of weak ion-sound damping ($T_i/T_e = 0.01$, $m_i/m_e = 183.6$) to avoid suppressing S-T coupling.[24,25] Previous EMSPT simulations that did not

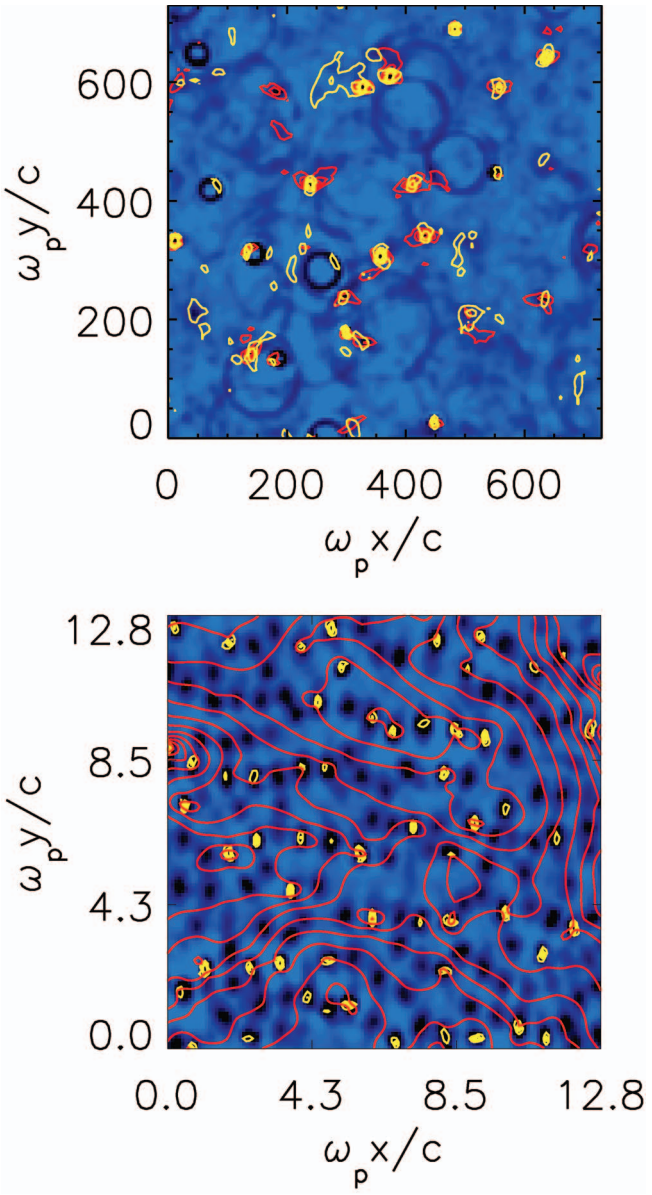

FIG. 1. (Color) EMSPT plots from the central part of the simulation box for (a) $v=0.57$ and (b) $v=0.01$, showing $\delta n/n_0$ (blue scale; dark negative, light positive, with a typical range from circa −0.4 at burnout to 0.1 W between packets, as in Ref. 13), $W_L=2,4,6,8,10\times10^{-3}$ (yellow contours), and $W_T=2,4,6,8,10\times10^{-3}$ (red).

average over fast oscillations in (1) and (2) showed that T power at $2\omega_p$ and $3\omega_p$ has only weak or negligible back reaction on the ω_p dynamics,[21] so we ignore T waves at harmonics of ω_p. Neglect of harmonics is also implicit in the derivation of the Zakharov equations themselves. We solve (1) and (2) using a spectral code with periodic boundary conditions, verifying that it correctly simulates linear wave propagation, ES parametric decays, and ESSPT (Refs. 10, 12, and 13) when the T waves are artificially suppressed.

Figure 1 depicts steady-state EMSPT for (a) $v=0.57c$ and (b) $v=0.01c$, via contours of $W_{L,T}=\epsilon_0|\mathcal{E}_{L,T}|^2/4n_0k_BT_e$. In both cases, the two-component spatial structure typical of SPT is evident: a sea of low-level, incoherent, delocalized waves (free modes) is punctuated by intense, coherent wave packets (trapped modes), which nucleate in pre-existing density wells and collapse to short scales and high fields via ponderomotive self-focusing.[10] The L waves are trapped for all v, but T waves delocalize for $v\lesssim0.1c$, forming long-wavelength clumps that are larger than, and do not coincide with, individual density wells, except possibly the sites of the most intense collapses. This new phenomenon is discussed further below, and does not occur in ESSPT. In Fig. 1(b), for $v\gtrsim0.1c$, overlapping, expanding, ring-like density depressions exist throughout the box. Each ring is a relic of a circular S wave launched by a wave packet in the final stage of collapse. Similar rings were seen in simulations of clamp-driven ESSPT, for $T_i\ll T_e$ but were peanut-shaped.[24,25]

Trapped and free modes in Figs 1(a) and 1(b) approximately satisfy the Schrödinger equation $i\partial_t|\rangle=\hat{Z}|\rangle$, where $|\,\rangle$ denotes the vector electric field and $\hat{Z}$ is the operator in parentheses in (1) with δn fixed and $\hat{\gamma}_L=0$. As $\hat{Z}$ does not depend explicitly on t, $|\,\rangle$ can be expanded as a sum $|\rangle=\Sigma_m c_m|m\rangle e^{-i\omega_m t}$ of time-independent eigenmodes with $\hat{Z}|m\rangle=\omega_m|m\rangle$. By numerically decomposing trapped modes in Figs 1(a) and 1(b) into 2D multipole harmonics $\Phi^{(m)}\propto e^{im\phi}$, we find they are chiefly dipolar, with $|L,m\rangle=-\nabla\Phi^{(m)}$, $|T,m\rangle=\hat{\mathbf{z}}\times\nabla\Phi^{(m)}$, and $\Phi_{L,T}^{(\pm1)}\propto(1+r^2/a_{L,T}^2)^{-1}re^{\pm i\phi}$, having peanut-shaped W_L and W_T contours with perpendicular major axes. The half-widths of the autocorrelation functions of the L and T fields, satisfy $a_L\approx a$ and $a_T\approx1.0(c/v)^{0.7}a$, where a is the length scale of the density well. Within uncertainties over the range investigated, these results are consistent with $a_T\approx ca_L/v\sqrt{3}$, as expected if the $\nabla\times\nabla\times$ and $\nabla\nabla\cdot$ terms in (1) are comparable and $|\Phi_L|\approx|\Phi_T|$. The density well is roughly circular, with a fit $\delta n(r)\propto(1+r^2/a^2)^{-2}$, as expected under subsonic conditions ($\partial_t^2\ll v_S^2\nabla^2$, $\delta n\propto|\mathcal{E}|^2$).[10]

Trapped T states cannot exist for low v because T dispersion overcomes refraction into density wells dug by trapped L waves. The (degenerate) eigenvalue of a trapped, dipole ($m=\pm1$) T mode is $\omega_{T,\pm1}/\omega_p=4c^2\lambda_D^2/v^2a_T^2+\delta n(0)/2n_0$. Using the empirical result $\delta n(0)/n_0\approx-31\lambda_D^2/a_L^2$, with a_T as above, we find $\omega_{T,\pm1}>0$ (detrapping) for $v<0.13c$. [The L eigenvalue $\omega_{L,\pm1}/\omega_p=12\lambda_D^2/a_L^2+\delta n(0)/2n_0$, is negative for all v.] This explains the delocalized structure of T modes in Fig. 1(b); W_T contours meander through the box, slightly favoring centers of density wells. Numerically decomposing the free T modes into 2D multipoles, we find the $|m|\geqslant2$ components have amplitudes comparable to the noise; they approximate plane waves ($\omega_{T,\mathbf{k}}=c^2k^2/2\omega_p$).

Figure 2(a) displays W_L and W_T versus t for $v=0.1c$. We initialize $\mathcal{E}(\mathbf{x},0)$ with curl-free noise with a k^{-2} spectrum to mimic the $k\approx0$ condensate of a parametric cascade, and set $\delta n(\mathbf{x},0)=0$.[10] Initial rises in W_L and W_T mark a plane-wave modulational instability, in which the condensate converts into a single, large wave packet that fills the simulation then collapses. The e-folding time of W_L is twice that of W_T (second-order process); growth takes place on the ponderomotive time scale $(W_L\omega_p)^{-1}$ and even faster if $\delta n<0$ initially (more k-matched decay channels available).[1–3] Similar behavior is seen in undriven simulations for similar parameters ($v=0.079c$) but in different initial conditions (e.g., single packet).[21]

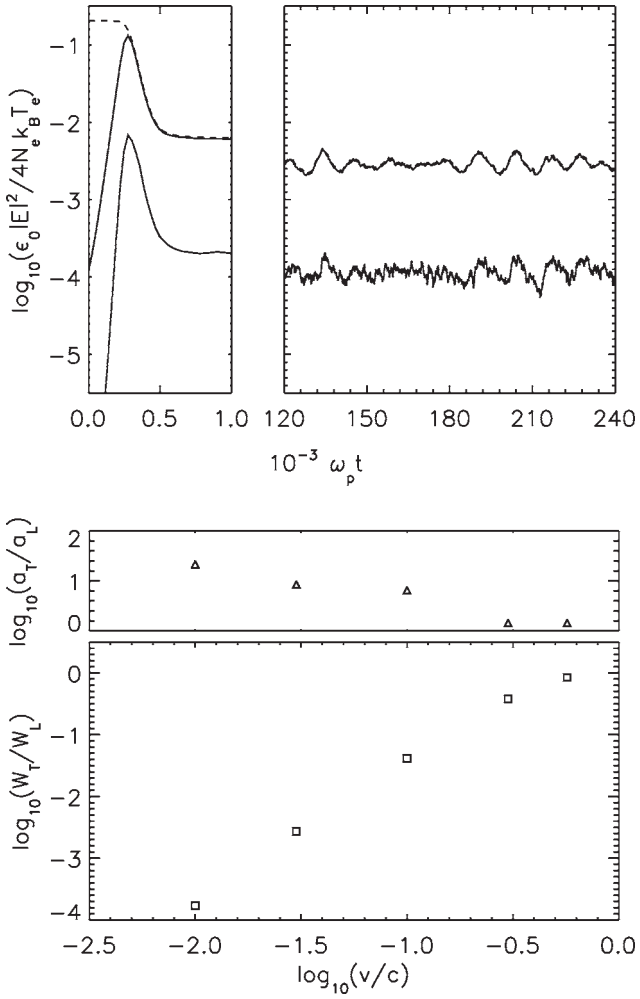

FIG. 2. (a) Wave-energy density: total W (dashed), W_L (top solid curve), and W_T (lower solid curve). Left panel shows initial modulational instability; right shows steady state EMSPT. (b) W_T/W_L (squares) and a_T/a_L (triangles).

Once the initial modulational instability saturates, at $t \approx 400\omega_p^{-1}$ in Fig. 2(a), memory of the condensate is lost and steady-state turbulence is maintained by a negative damping driver at $(\omega_b, \mathbf{k}_b) = (\omega_p, 0)$, of width $\Delta k_b = 2k_{\max}/N$ and peak growth given by $\gamma_L = -10^{-3}\omega_p$, where $k_{\max}$ is the maximum k and N is the number of grid units along each axis.[10] Previous EMSPT simulations were undriven and did not attain a steady state.[17,21] We choose $k_{\max} = 0.31\lambda_D^{-1}$ and time step $\Delta t \leq 2.1\omega_p^{-1}(v/c)^2$ to follow the fast $\nabla \times \nabla \times$ term in (1). Damping occurs at a rate $\gamma_L = \gamma_0(k) + a[(k/k_c)^2 - 1]$, with $a = 0.04\omega_p$ and $k_c = 0.8k_{\max}$; the first term is linear Landau damping, the second a proxy for coherent transit-time damping, which is set to zero for $k < k_c$.[10]

A prominent feature of Fig. 2(a), absent from ESSPT driven at $k \approx 0$, is the existence of quasiperiodic, long-period cycles in W_L and W_T, with period $T_{LT} = (1.2 \pm 0.2) \times 10^4 \omega_p^{-1}$, and similar fractional amplitudes (factors of up to ~ 2 and ~ 4, peak to trough, for L and T, respectively, with this $\sim 2:1$ ratio consistent with nonlinear generation of T waves). They intermittently die out and re-emerge, persisting for $> 50T_{LT}$. (These global cycles are not the same as the nucleation cycles seen at individual collapse sites,[10,12,24] which are also observed here.) On cross-correlating the time series, one finds that W_L lags W_T by $\Delta T_{LT} = (7.7 \pm 1.1) \times 10^2 \omega_p^{-1}$, comparable to the ponderomotive (i.e., modulational) time scale $(W_L\omega_p)^{-1}$. The period T_{LT} varies by less than 20% over the range $0.01c \leq v \leq 0.57c$ [i.e., $v_T \approx v_L$ at the upper bound, where $c/\sqrt{3} \approx 0.57c$ is the sound speed in a relativistic gas; the lower bound is set by the point where $k^2 v_T^2$ becomes large, as seen in Fig. 3(a)], does not depend on box size, and

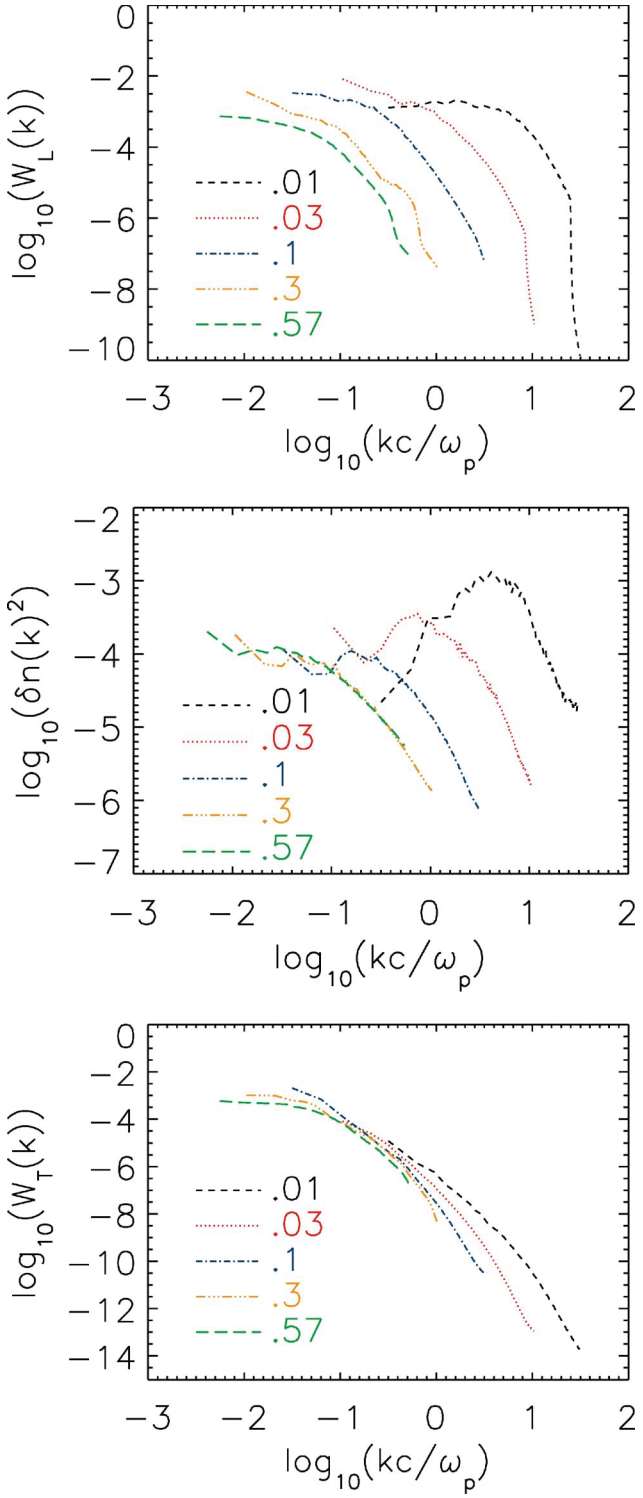

FIG. 3. Angle-averaged spectra (arbitrary units) for $v/c = 0.01, 0.03, 0.1, 0.3, 0.57$. (a) $\langle|\mathcal{E}_L(\mathbf{k})|^2\rangle$, (b) $\langle|\delta n(\mathbf{k})|^2\rangle$, and (c) $\langle|\mathcal{E}_T(\mathbf{k})|^2\rangle$. Spectra are averaged over a time $5 \times 10^4 \omega_p^{-1}$.

is ≈20 times longer than the growth times of (i) ES three-wave decay,[10] (ii) EM modulational instability $L+L\rightarrow T+T$,[26,27] and (iii) sloshing between the mixed L-T normal modes of an inhomogeneous plasma. As these cycles are absent from ESSPT, they likely involve 3- or 4-wave coupling of L and T modes.

Figure 2(b) shows the mean steady-state value of W_T/W_L versus v (excluding the $k=0$ mode, which contains ≈2% of the total energy), with a_T/a_L also plotted for reference. Least-squares fits yield $W_T/W_L \propto v^{2.4\pm0.1}$ ($v \lesssim 0.1c$) and $W_T/W_L \propto v^{1.2\pm0.1}$ ($v \gtrsim 0.1c$); the proportionality constants are functions of the driver and damping. However, when underestimates of the low-k part of the spectrum [see Fig. 3(c), where the lower bound to each curve is determined by the box size] are taken into account, the results are consistent with $W_T/W_L \sim v^{1.8}$ over the whole range investigated. We also obtain $W_L \propto v^{-0.67\pm0.03} \propto (\Delta k_b)^{0.67}$, in accord with Eq. (6.20) of Ref. 10 for 2D ESSPT.

Wave number spectra $W_{LT}(k)=\langle|\mathcal{E}_{LT}(\mathbf{k})|^2\rangle$ and $\delta n(k)^2 = \langle|\delta n(\mathbf{k})|^2\rangle$, averaged over time and angle, are shown in Fig. 3. For $v \lesssim 0.1c$, we find power-law inertial ranges at $k_n \lesssim k \lesssim k_c$, with $k_n = \pi/a_L = 0.66 W^{1/2}\lambda_D^{-1}$, $W_L(k) \propto k^{-3.9\pm0.4}$, $\delta n(k)^2 \propto k^{-2.3\pm0.5}$, and $W_T(k) \propto k^{-5.8\pm0.8}$. [For our parameters, the minimum nonzero k at the left end of each curve in Fig. 3(a) is at $k_{\min}c/\omega_p \approx 0.003c/v$, the beginning of the inertial range at the right end of the shallowly sloped part of each curve is at $k_n c/\omega_p \approx 0.04c/v$, the upper bound of each curve is at $k_{\max}c/\omega_p \approx 0.35c/v \approx 1.25k_c c/\omega_p$, where k_c is the upper bound of the Langmuir inertial range.] The latter scaling is new, while the first two agree with the two-component theory of 2D ESSPT, which predicts $W_L(k) \propto k^{-4}$ and $\delta n(k)^2 \propto k^{-2}$.[10,12,13] Although we have $W_T \ll W_L$ overall, we find $W_T(k) \sim W_L(k)$ for $k_b \lesssim k \lesssim k_n$, where T waves are generated by weak turbulence processes that partition energy roughly equally between modes.

For $v \gtrsim 0.1c$, a slight bump interrupts the inertial range of $W_L(k)$ at $k_T = \pi/a_T \approx 0.2(v/c)^{-0.33}\omega_p/c$. (Most T waves are generated near when collapse arrests at $a_L \approx 15\lambda_D$.) We find $k_n < k_T < k_c$ for $v \gtrsim 0.1c$. The bump also exists for $v \lesssim 0.1c$, but falls outside the inertial range ($k_T < k_n$). It may mark enhanced focusing of L waves into density wells, deepened by the additional ponderomotive force of the T waves, but it is unclear why there is no bump in $W_T(k)$. T waves are not damped directly, but are converted to damped L and S waves via 3- and 4-wave processes. Indirect T damping explains the (i) absence of a sharp cutoff in $W_T(k)$ at k_c, because the damping operates at all k, and (ii) sensitivity of W_T, but not W_L, to $\hat{\gamma}_S$, which affects the steady-state level of S waves. The gradual decline of $W_T(k)$ above k_c is due to the shortage of k-matched L waves converting to T waves.

Several potential applications are flagged above. One is to interpret particle-in-cell (PIC) simulations of ultrashort, relativistic laser pulses propagating into an underdense plasma, where 30%–40% of the incident energy is transformed into "solitons" behind the pulse.[6–8] The group velocity of most solitons is negligible, consistent with wave packets in Fig. 1 and ESSPT (Ref. 10) (although in some PIC simulations[7] solitons drift backwards at $0.3-0.8c$). Solitons nucleate in laser-generated channels, then collapse. After collapse is arrested, the fields relax to fill slowly expanding, ring-like density cavities which trap T modes.[9,28] This behavior closely matches that of the density depressions in Fig. 1(b).

Good prospects also exist to test our predictions in other laboratory situations; e.g., when packets containing coupled L and T modes [see Fig. 1(a)] approach a plasma-vacuum interface, they radiate a burst of EM waves, whose spectrum reflects the field structure of the packet and hence $W_T(k)$.[7] As this structure changes at $v=0.1c$, it is possible in principle to detect the delocalization transition with this diagnostic. In addition, we only expect to see ring-like postsolitons for $v \geqslant 0.1c$. This ability to infer some parameters of SPT (e.g., v, W_L) from remote measurements is also potentially useful in astrophysics[14–17] and laboratory experiments demanding noninvasive diagnostics.

ACKNOWLEDGMENTS

The NSF, NASA, Miller Institute for Basic Research in Science, Australian Research Council, and Caltech Center for Advanced Computing and Research supported this work.

[1] D. A. Whelan and R. L. Stenzel, Phys. Rev. Lett. **47**, 95 (1981).
[2] P. Y. Cheung, A. Y. Wong, C. B. Darrow, and S. J. Qian, Phys. Rev. Lett. **48**, 1348 (1982).
[3] M. Schneider and M. Q. Tran, Phys. Lett. **91A**, 25 (1982).
[4] E. Mjølhus, A. Hanssen, and D. F. DuBois, J. Geophys. Res. **100**, 17527 (1995).
[5] P. Y. Cheung, E. Mjølhus, D. F. DuBois, J. Pau, H. Zwi, and A. Y. Wong, Phys. Rev. Lett. **79**, 1273 (1997).
[6] S. V. Bulanov, T. Zh. Esirkepov, N. M. Naumova, F. Pegoraro, and V. A. Vshivkov, Phys. Rev. Lett. **82**, 3440 (1999).
[7] Y. Sentoku, T. Zh. Esirkepov, K. Mima, K. Nishihara, F. Califano, F. Pegoraro, H. Sakagami, Y. Kitagawa, N. M. Naumova, and S. V. Bulanov, Phys. Rev. Lett. **83**, 3434 (1999).
[8] K. Mima, M. S. Jovanović, Y. Sentoku, Z.-M. Sheng, M. M. Škorić, and T. Sato, Phys. Plasmas **8**, 2349 (2001).
[9] D. Umstadter, J. Phys. D **36**, R151 (2003).
[10] P. A. Robinson, Rev. Mod. Phys. **69**, 507 (1997), and references therein.
[11] A. Melatos and P. A. Robinson, Phys. Fluids B **5**, 1045 (1993).
[12] P. A. Robinson and D. L. Newman, Phys. Fluids B **2**, 2999 (1990).
[13] P. A. Robinson and D. L. Newman, Phys. Fluids B **2**, 3017 (1990).
[14] H. P. Freund and K. Papadopoulos, Phys. Fluids **23**, 732 (1980).
[15] M. V. Goldman, G. F. Reiter, and D. R. Nicholson, Phys. Fluids **23**, 388 (1980).
[16] B. Hafizi and M. V. Goldman, Phys. Fluids **24**, 145 (1981).
[17] J. Weatherall, Astrophys. J. **483**, 402 (1997).
[18] J. Gibbons, S. G. Thornhill, M. J. Wardrop, and D. ter Haar, J. Plasma Phys. **17**, 153 (1977).
[19] M. Kono, M. M. Škorić, and D. ter Haar, J. Plasma Phys. **26**, 123 (1981).
[20] P. L. Pritchett and J. M. Dawson, Phys. Fluids **26**, 1114 (1983).
[21] K. Akimoto, H. L. Rowland, and K. Papadopoulos, Phys. Fluids **31**, 2185 (1988).
[22] L. H. Li, Phys. Fluids B **5**, 350 (1993).
[23] A. Magneville, J. Plasma Phys. **44**, 191 (1990).
[24] G. D. Doolen, D. F. DuBois, and H. A. Rose, Phys. Rev. Lett. **54**, 804 (1985).
[25] D. Russell, D. F. DuBois, and H. A. Rose, Phys. Rev. Lett. **60**, 581 (1988).
[26] K. Akimoto, Phys. Fluids **31**, 538 (1988).
[27] F. B. Rizzato and A. C.-L. Chian, J. Plasma Phys. **48**, 71 (1992).
[28] N. M. Naumova, S. V. Bulanov, T. Zh. Esirkepov, D. Farina, K. Nishihara, F. Pegoraro, H. Ruhl, and A. S. Sakharov, Phys. Rev. Lett. **87**, 185004 (2001).